Masked least-squares averaging in processing of scanning-EMG recordings with multiple-discharges

Íñigo Corera · Armando Malanda · Javier Rodríguez-Falces · Javier Navallas

Total number of words of the manuscript: 6831

Number of words of the abstract: 197

Number of figures: 8

Number of tables: 0

The authors are with the Department of Electrical, Electronic and Communication Engineering, Public University of Navarra, 31006 Navarra, Spain (e-mail: inigo.corera@unavarra.es)

Abstract

Removing artifacts from nearby motor units is one of the main objectives when processing scanning-EMG recordings. Methods such as median filtering or masked least-squares smoothing (MLSS) can be used to eliminate artifacts in recordings with just one discharge of the motor unit potential (MUP) at each location. However, more effective artifact removal can be achieved if several discharges per position are recorded. In this case, processing usually involves averaging the discharges available at each position and then applying a median filter in the spatial dimension. The main drawback of this approach is that the median filter tends to distort the signal waveform. In this paper, we present a new algorithm that operates on multiple discharges simultaneously and in the spatial dimension. We refer to this algorithm as the multi masked least-squares smoothing (MMLSS) algorithm: an extension of the MLSS algorithm for the case of multiple discharges. The algorithm is tested using simulated scanning-EMG signals in different recording conditions, i.e., at different levels of muscle contraction and for different numbers of discharges per position. Results demonstrate that the algorithm eliminates artifacts more effectively than any previously available method and does so without distorting the waveform of the signal.

Keywords: Electromyography · Scanning-EMG · Signal processing · Motor unit

1-Introduction

The scanning-EMG technique consists in recording the electrical activity of the motor unit (MU) at multiple locations throughout the motor unit territory [31]. A modified implementation of this technique makes it possible, in a single scan, to simultaneously record the electrical activity of not only one, but several MUs [38, 18, 28]. This has enabled study of the overlapping of MU territories within the muscle [38, 18]. The scanning-EMG technique is also useful for investigating the organization of muscle fibres within the MU territory [7, 12, 24, 31, 34] and for studying neuromuscular pathologies [7, 10, 11, 12, 14, 15, 35, 2].

Analysis of a scanning-EMG signal usually consists on extracting several parameters from the signal, such as, the length of the MU territory [12], or some parameters concerning fractions (high amplitude signal regions separated in time or space by low amplitude signal regions (<50 μV) [35]) and silent zones (signal regions with very low amplitude), being the most relevant ones the number and length of fractions [35], the number and length of polyphasic fractions [35], the temporal delay between fractions [24], and the number and length of silent

zones [35]. An alternative parametrization to analyse the scanning-EMG signal is the motor unit profile [4].

The scanning-EMG signal comprises a collection of motor unit potentials (MUPs) from a certain MU recorded, using a needle electrode, in different positions at different depths within the muscle. The recording can be configured to obtain either one or several discharges of the MUP at each position of the needle. When multiple discharges are recorded per position, the scanning-EMG signal has three dimensions (Fig. 1): the temporal dimension, since each MUP discharge is a signal varying with time; the spatial dimension, i.e., the different recording positions; and the discharge dimension.

A raw scanning-EMG signal will usually be contaminated with different types of noise, the most troublesome of which is interference deriving from the activation of nearby MUs during the recording of the MUP [12, 13, 27]. This phenomenon results in a large number of artifacts - electrical activity that is not synchronized with the firing of the MU being tracked - superimposed on the recorded MUP [27] (Figs. 1 and 2 (a)).

This kind of noise needs to be eliminated before the signal analysis, and various techniques have been used for this purpose. All of these techniques are based on the observation that artifacts, because they are not synchronized with the firing of the MU under study, are not repeated regularly in time throughout the series of recorded MUP discharges. This means that, both in the spatial and in the discharge dimension, artifacts are effectively impulsive noise, and it is this fact that is exploited by the processing techniques.

When only a single discharge of the MUP is recorded at each position, the strategy used to eliminate artifacts is to filter in the spatial dimension (Fig. 2 (b)). Traditionally, the median filter (usually of 3, 5 or 7 points) [12, 13, 27] has been used for this purpose. However, this filter noticeably distorts the waveform of the scanning signal. Phenomena such as peak clipping [12, 13, 27] or stepping of the amplitude profile in the spatial dimension [5] have been reported when the median filter is used. A useful alternative to median filtering is the masked least-squares smoothing (MLSS) algorithm [5], which eliminates artifacts but preserves the signal waveform noticeably better than the median filter.

When multiple MUP discharges per position are recorded, artifacts can be removed by averaging (using the mean or median) the different discharges existing at each position [33]. This strategy is well-known in quantitative electromyography (EMG), where it is used to extract

representative MUP waveforms, and several averaging algorithms, such as, [3, 32, 1, 16, 23, 36, 22, 20, 19, 21] have been developed.

With multi-discharge scanning-EMG recordings, artifact elimination is more effective if the averaging is applied not only for the various discharges at each position, but also in the spatial dimension. In [38], the discharges at each recording position are averaged, and then a spatial median filter is applied. However, this approach has two main drawbacks: the first one is that it is based on the median filter, and therefore tends to result in peak clipping and stepping of the amplitude profile; and the second one is that it performs the two processing stages sequentially, which is less effective than operating simultaneously in both dimensions.

The aim of the present work is to present a new algorithm to remove the artifacts in multiple discharge scanning-EMG recordings. The algorithm operates simultaneously on the discharges recorded at each position and in the spatial dimension. We will refer to the process used by the algorithm, which is a development of MLSS, as multi masked least-squares smoothing (MMLSS). In this paper, the MMLSS algorithm is presented and described, and its ability to remove artifact noise in simulated scanning-EMG recordings is analysed and compared with that of previously available methods.

2-Materials and methods

2.1-Algorithm description

We assume that several MUP discharges are recorded at each spatial position (Fig. 3 (a)). Before applying the algorithm itself, each discharge can be processed with a temporal band-pass filter so as to eliminate baseline and instrumentation noise [27]. The MMLSS algorithm has three main steps: artifact detection, discharge averaging, and least-squares smoothing (Fig. 4).

2.1.1-Artifact detection

The first step of the algorithm is to detect, for each of the recorded discharges, which samples of recorded data are contaminated with artifacts (Fig. 4). To this end, artifact noise is estimated by computing the difference between the sample values of the input scanning signal and the sample values of a calculated median-filtered signal. Then, contaminated, i.e. invalid, samples are determined by thresholding the estimated artifact noise.

Let $\boldsymbol{X} = \{x_{n,k}^{j}\}$ be the scanning-EMG signal at the input of the algorithm, where $1 \leq n \leq N$ and $1 \leq k \leq K$ are the temporal and spatial location of the sample respectively, and $1 \leq j \leq J(k)$ the discharge to which the sample belongs, where N and K are the number of temporal and spatial samples of the scanning signal respectively, and $J(k)$ is the number of discharges recorded in the position k.

Computing the median-filtered signal $\boldsymbol{G} = \{g_{n,k}\}$ consists on applying a median filter, then mean subtraction of each trace, and finally a second median filter. The aim of double median filtering is to improve artifact removal; the mean subtraction step helps to eliminate the bias of any remaining artifact noise.

To obtain the filtered value at each space-time position (n, k), the first filter computes the median of all sample values contained within a window of L spatial positions centered at (n, k) (Fig. 3 (a-b)). Notice that several sample values, corresponding to the different discharges, may exist at each spatial position of the window. In this way this first median filter is operating simultaneously among the spatial and discharge dimensions, namely

$$g_{n,k} = \text{median}\{x_{n,k+l}^{j} \mid 1 \leq j \leq J(k), -(L-1)/2 \leq l \leq (L-1)/2\} \quad (1)$$

where the size of signal $\boldsymbol{G}$ is $N \times K$, as the different discharges existing at each specific space-time position have been combined into a single value. Once the first median filter is applied, the mean of each trace at each spatial position is subtracted, and then, a second L-point median filter is applied along the spatial dimension

$$g_{n,k} = \text{median}\{g_{n,k+l} \mid -(L-1)/2 \leq l \leq (L-1)/2\} \quad (2)$$

The validity mask, $\boldsymbol{V} = \{v_{n,k}^{j}\}$, is obtained by thresholding the difference between the input signal, $\boldsymbol{X}$, and the median-filtered signal, $\boldsymbol{G}$ (Fig. 3 (c)). The mask is set to 1 indicating that an artifact has not been detected and 0 otherwise (Fig. 3 (d))

$$v_{n,k}^{j} = \begin{cases} 1 & \left|x_{n,k}^{j} - g_{n,k}\right| < U \cdot (\max(G) - \min(G)) \\ 0 & \left|x_{n,k}^{j} - g_{n,k}\right| \geq U \cdot (\max(G) - \min(G)) \end{cases} \quad (3)$$

where U is the normalized artifact detection threshold. Note that there is a one-to-one correspondence between the sample points of the input scanning signal, $\boldsymbol{X}$, and those of the validity mask, $\boldsymbol{V}$, (Fig. 3 (a) and (d)), thus these matrices have the same size.

2.1.2-Discharge averaging

The second step of the algorithm is to combine the information of the different discharges at each space-time position. An overall validity mask, $\boldsymbol{W} = \{w_{n,k}\}$, indicating the number of valid samples at each position is created by summing, at each position (n, k), all the validity mask values associated with the different discharges (Fig. 4)

$$w_{n,k} = \sum_{j=1}^{J(k)} v_{n,k}^{j} \quad (4)$$

When it comes to building the output signal in the least-squares smoothing step (see section 2.1.3), the overall validity mask will be used to give to each position a weight proportional to the number of valid samples detected.

An averaged scanning signal, $\boldsymbol{F} = \{f_{n,k}\}$, is obtained from the input scanning signal by averaging the samples of the different discharges at each position (n, k) weighted by the validity mask (Fig. 4)

$$f_{n,k} = \begin{cases} \dfrac{\sum_{j=1}^{J(k)} v_{n,k}^{j}\, x_{n,k}^{j}}{w_{n,k}} & w_{n,k} > 0 \\ 0 & w_{n,k} = 0 \end{cases} \quad (5)$$

Note that this ensures that the averaged signal contains only the information of artifact-free samples, because invalid samples are given a weight of 0 in the averaging procedure.

2.1.3-Least squares smoothing

The third and last step of the algorithm is to build the output scanning signal by applying least-squares smoothing to the averaged signal (Fig. 4). For each space-time position (n, k), a polynomial of order Q is fitted to the amplitude values of the samples contained in a window of length $2M + 1$, selected along the spatial dimension and centered at the position under consideration. The criteria used for the polynomial fitting is weighted linear least-squares [37], where the weights are the overall validity mask values. In this way, the $N \times K$ output scanning signal, $\boldsymbol{Y} = \{y_{n,k}\}$, is composed of the values of the calculated polynomials at the centre of the windows [5]. Therefore, at each position (n, k), the output value is

$$y_{n,k} = \beta_0 \quad (6)$$

where the coefficients of the polynomial $\boldsymbol{\beta} = \left[\beta_0, \cdots, \beta_Q\right]^T$ are calculated as [37]

$$\boldsymbol{\beta} = (\boldsymbol{S}^T \boldsymbol{A} \boldsymbol{S})^{-1} \boldsymbol{S}^T \boldsymbol{A} \boldsymbol{f} \tag{7}$$

where $\boldsymbol{f} = \left[f_{n,k-M}, \cdots, f_{n,k}, \cdots, f_{n,k+M}\right]^T$ are the samples values within the window, the weight matrix $\boldsymbol{A}$ is a diagonal matrix built from the overall validity mask values matched to the positions within the window

$$\boldsymbol{A} = \mathrm{diag}\{w_{n,k-M}, \cdots, w_{n,k}, \cdots, w_{n,k+M}\}, \tag{8}$$

and the matrix $\boldsymbol{S}$ is defined as

$$\boldsymbol{S} = \{s_{q,m}\}, \quad s_{q,m} = \begin{cases} m^q & q \neq 0 \\ 1 & q = 0 \end{cases} \tag{9}$$

where $-M \leq m \leq M$ and $0 \leq q \leq Q$. Note that the weight matrix $\boldsymbol{A}$, the window sample values $\boldsymbol{f}$, and the polynomial coefficients $\boldsymbol{\beta}$ (and therefore also β_0), are calculated for every space-time position (n, k), although this dependency has not been explicitly indicated in the equations.

For spatial positions near to the edges of the scanning signal, where there do not exist M traces on each side, the output is calculated as described in [5].

As noted in [5], the value of the polynomial order must be restricted in some space-time positions. This restriction avoids incorrect polynomial solutions that can arise if the polynomial order is high relative to the number of samples used. The condition applied is

$$Q < \frac{1}{2} \sum_{m=-M}^{M} \mathfrak{u}_m \tag{10}$$

where

$$\mathfrak{u}_m = \begin{cases} 1 & w_{n,k} > 0 \\ 0 & w_{n,k} = 0 \end{cases} \tag{11}$$

For space-time positions at which this condition is not satisfied, the highest polynomial order Q that does satisfy the condition is chosen.

Once the scanning signal, $\boldsymbol{Y}$, has been obtained, the mean of each trace at each spatial position is subtracted to eliminate the bias of the remaining noise.

2.2-Algorithm evaluation

2.2.1-Model of scanning-EMG signals

Simulated scanning-EMG signals were used in order to evaluate the performance of the MMLSS algorithm. The complete model for simulating scanning-EMG signals comprises several sub-models, all of them described in detail in [5].

Model of muscle and MU. The muscle was modelled with a circular cross section of 10 mm diameter composed of 120 MUs [5]. The cross-sectional areas of MUs were distributed with an exponential function [9], with the smallest MU area being 1.96 mm^2, and the largest one 22.48 mm^2. MU territories were modelled circular in shape in agreement with [17, 24, 25]. Territories were placed within the muscle cross section so as to minimize the variance of the overlapping of the territories [25, 30]. The muscle fibres within each MU were distributed uniformly [8], with a fibre density of 10 fibres/mm^2. The conduction velocity of the muscle fibres followed a Gaussian distribution whose mean varied among the different MUs according to an exponential function [9], with the smallest MU having a mean conduction velocity of 3.25 m/s, and the largest one of 6.25 m/s, and whose coefficient of variation was 0.03. The innervation zone and the innervation position of MU fibres were modelled to emulate MU fractions following [5]. In a first step, the muscle cross section was randomly divided in 90 different regions (MU fractions) by means of a Voronoi tessellation. Then, for each MU, the innervation positions of its fibres belonging to a certain MU fraction were uniformly distributed within a 1 mm wide region (innervation sub-band) [5]. The position of these sub-bands was uniformly distributed within the overall innervation zone, which was 10 mm wide, and was located in the middle of the muscle, lengthwise [5].

Model of the recruitment and firing pattern. The recruitment threshold of the different MUs during constant isometric contraction was modelled by an exponential function [8, 9], where the percentage of full recruitment was 70% [9]. The firing rate of the MUs was modelled as described in [8]. Firing rate increased linearly with increased percentage of voluntary contraction: an increment of 7 pulses per second for each 10% increase in the maximum voluntary contraction (MVC). The minimum and maximum firing rate was 8 and 35 pulses per second, respectively [8]. The firing pattern of each MU was modelled as a renewal point

process [8]. The interval between discharges followed a Gaussian distribution whose mean was the inverse of the firing rate, and whose coefficient of variation was 0.15.

Model of the scanning-EMG signal. MUPs recorded with a concentric needle were modelled following [6, 29]. The time duration of the MUPs was 30 ms, and the sampling frequency 20 kHz. The physiological (noise-free) scanning-EMG signal was simulated as the sequence of MUPs simulated at each position of the needle [5]. The needle was inserted in the middle of the muscle in the muscle cross section plane; and 30 mm away from the innervation zone in the fibre direction. The recording positions taken by the needle comprised a linear corridor extending from the deepest part of the muscle to the shallowest in steps of 0.05 mm.

The recording procedure of the scanning-EMG signal was modelled in order to obtain realistic signals in which noise and artifacts deriving from other MUs are present. At each position of the needle electrode, the convolution of the MUPs of all recruited MUs by the firing trains was calculated to obtain the complete EMG signal [5], and the recorded MUP discharges associated with the different MU firing times was extracted from this signal. The entire scanning signal was obtained by repeating this procedure at each recording position. The time interval that the electrode remained at each specific recording position was set to ensure a specific number of MUP discharges. The baseline was modelled as an ARMA process [26] by filtering white Gaussian noise of zero mean and 3.5 mV standard deviation with a low-pass filter. The filter used was a 5th-order Butterworth low-pass filter with a 3-dB cut-off frequency of 20 Hz. Instrumentation noise was simulated as a zero-mean additive white Gaussian noise process, with a standard deviation of 0.035 mV.

2.2.2-Experiments with simulated signals

Scanning-EMG signals were simulated in different recording scenarios. We evaluated different levels of activation of the muscle: 2%, 4%, 8% and 20% of the MVC which correspond to 19, 39, 58 and 84 recruited MUs respectively. Different degrees of muscle contraction imply different levels of artifact contamination. In addition, we studied the influence of the number of discharges recorded at each position of the scanning electrode, with simulations comprising 1, 3, 5 and 7 discharges. For each case, 20 independent muscle realizations were simulated. Note that the arrangement of the MUs within the muscle, and the specific parameters of each individual muscle fibre are different for each simulation run of the muscle. For each muscle realization, one scanning signal was obtained for each of the MUs whose territory was traversed by the scanning electrode (Fig. 5).

The MMLSS algorithm was tested and compared with other algorithms typically used in scanning-EMG recordings. Each signal was processed with the MMLSS algorithm using the following operating parameters: median filter order, L = 5; artifact detection threshold, U = 3 · 10^{-2}; polynomial order, Q = 8; and window semi-length, W = 13. Optimal parameter values were obtained following the optimization procedure described in [5] (note that both the MLSS and the MMLSS algorithms share the L, U, Q and W parameters). This procedure consisted in minimizing the error power of the processed signal for 100 simulation runs by means of a genetic algorithm [5]. The parameter values obtained for the MMLSS are very close to the optimal values obtained in [5] for the MLSS operating parameters.

Additionally, the signals were processed with different median filter-based algorithms, all of which first averaged the different discharges at each recording position, and then applied a median filter in the spatial dimension [38]. Algorithms using discharge averaging based on the mean, will be referred to as mean-median algorithms; those using discharge averaging based on the median, will be referred to as median-median algorithms. In both cases, three different numbers of points (3, 5 and 7 points) were used for the spatial median filter. Therefore, a total of six median filter-based algorithms were used: the mean and 3 point median (m-M3), the mean and 5 point median (m-M5), the mean and 7 point median (m-M7), the median and 3 point median (M-M3), the median and 5 point median (M-M5) and the median and 7 point median (M-M7).

For experiments with only one discharge per position, note that the mean-median and the median-median algorithms are identical, consisting only in application of a spatial median filter, as no discharge averaging is performed in this case. Therefore, a total of three median-filter based algorithms were used: the 3 point median (M3), the 5 point median (M5) and the 7 point median (M7). Analogously, with only one discharge per position, the MMLSS algorithm is equivalent to the MLSS [5].

For each processed signal, the error power within the physiological active region [5], P, was calculated

$$P = 10\log_{10}\frac{\sum_{k=1}^{K}\sum_{n=1}^{N} z_{n,k}\left|y_{n,k} - s_{n,k}\right|^2}{\sum_{k=1}^{K}\sum_{n=1}^{N} z_{n,k}} \quad (12)$$

where $y_{n,k}$ is the processed scanning-EMG signal, and $s_{n,k}$ is the physiological (ideal noise-free) scanning-EMG signal. The mask $z_{n,k}$ indicates whether a space-time sample is inside the

physiological activity region of the signal (mask set to 1) or not (mask set to 0) [5]. For each trace at each spatial position k, the physiological activity region is defined as the sample interval between the first n_{a_k} and last sample n_{b_k} for which the signal exceeds 9% of the maximum amplitude value of the entire physiological scanning signal:

$$z_{n,k} = \begin{cases} 1 & n_{a_k} \leq n \leq n_{b_k} \\ 0 & \text{otherwise} \end{cases} \quad (13)$$

For each of the simulated scanning signals, the gain in performance of the MMLSS algorithm with respect to the other algorithms, $G_{algorithm}$, was defined as

$$G_{algorithm} = P(algorithm) - P(MMLSS) \quad (14)$$

3-Results

3.1-Error power for the MMLSS algorithm

The results of error power obtained for the MMLSS algorithm at different levels of muscle contraction and for different numbers of discharges are shown in Fig. 6. Note that, the larger the number of discharges used, the lower the error power. The use of seven discharges with respect to the use of just one reduces the median error power by approximately 9 dB. This reduction is practically the same irrespective of the level of muscle contraction. Also, with regard to muscle contraction, the higher the contraction level, the higher the error power. At 2% MVC, the median error power ranged between -32.40 dBm and -23.22 dBm; at 4%, between -23.32 and -14.20 dBm; at 8%, between -17.28 and -8.87 dBm; and at 20%, between -10.65 and -2.32 dBm.

3.2-Comparison with other methods

The gain in performance of the MMLSS algorithm relative to other algorithms was evaluated at the three different levels of muscle contraction and for different numbers of discharges. The results are shown in Fig. 7. Note that performance gain was positive in almost all comparisons and scenarios.

In the multi-discharge cases, the median gain ranged between 6.52 dB (20% MVC, 3 discharges) and 10.07 dB (2% MVC, 7 discharges) with respect to the m-M3 algorithm; between 4.40 dB (20% MVC, 3 discharges) and 9.35 dB (2% MVC, 7 discharges) with respect to

the m-M5; between 3.25 dB (20% MVC, 3 discharges) and 9.76 dB (2% MVC, 7 discharges) with respect to the m-M7; between 3.27 dB (2% MVC, 7 discharges) and 4.82 dB (4% MVC, 3 discharges) with respect to the M-M3; between 2.67 dB (20% MVC, 3 discharges) and 4.3 dB (2% MVC, 3 discharges) with respect to the M-M5; and between 1.60 dB (20% MVC, 3 discharges) and 5.48 dB (2% MVC, 3 discharges) with respect to the M-M7.

In the single-discharge cases, the median gain ranged between 4.69 dB (8% MVC) and 4.93 dB (20% MVC) with respect to the 3-point-median algorithm; between 2.10 dB (8% MVC) and 3.49 dB (2% MVC) with respect to the 5-point-median; and between 0.65 dB (20% MVC) and 3.93 dB (2% MVC) with respect to the 7-point-median.

The median-median algorithms performed better than the mean-median algorithms: in all the recording conditions studied, the MMLSS gain values were lower when calculated against the median-median algorithms than when calculated against the mean-median counterparts (Fig. 7)).

3.3-Case of use of the MMLSS algorithm

Figure 8 shows an example of a simulated scanning-EMG signal (five discharges at 4% MVC) processed by different algorithms. The signal processed with the MMLSS algorithm has a smoothed amplitude profile in the spatial dimension (Fig. 8 (c)), with a similar shape to that of the noise-free ideal signal (Fig. 8 (d)). The signal processed with the M-M5 algorithm has a distorted amplitude profile with a stepped waveform (Fig. 8 (b)). Accordingly, the error power of this signal relative to the ideal signal was higher than that of the MMLSS algorithm (-18.68 dBm for the M5, and -22.04 dBm for the MMLSS). The signal processed with the m-M5 algorithm also has a stepped amplitude profile in the spatial dimension, and artifact noise has not been removed completely (Fig. 8 (a)). The error power was -14.52 dB in this case.

4-Discussion

In the processing of scanning-EMG signals, in order that subsequent signal analysis can be performed correctly and accurately, it is essential to remove artifact superimpositions produced by the activation of nearby MUs [12, 13, 27]. The use of a processing algorithm that can handle multi-discharge as opposed to single-discharge recordings makes elimination of this kind of noise noticeably more workable. Here, we have presented and evaluated the MMLSS

algorithm, which is a development on the MLSS algorithm [5] and which has been designed to be able to process multi-discharge scanning-EMG recordings.

Test results presented in Section 3.2 indicate that the MMLSS algorithm removes artifact noise while preserving the physiological waveform of the scanning signal in a more effective way than any other previously used median filter-based method. The gain in performance achieved with the MMLSS is positive relative to all other algorithms tested, at all levels of muscle contraction studied and with all the numbers of discharges evaluated (Fig. 7). For single-discharge recordings, a similar conclusion concerning the advantages of the MLSS algorithm over the median algorithm has been previously reported in [5].

The effectiveness of the MMLSS algorithm in correctly removing artifact noise can be understood in a deeper way by looking at a specific case of the algorithm in use (see Section 3.3). When the algorithm is used to process multi-discharge scanning signals (Fig. 8 (c)), not only is the processed signal clear of artifacts but also the amplitude profile is smooth in shape; and furthermore, the processed signal closely resembles that of the ideal noise-free signal (P = -22.04 dBm). These observations further evidence that the MMLSS barely distorts the waveform of the scanning signal. Low distortion has been previously reported for the MLSS algorithm when processing single-discharge recordings [5]. The MMLSS algorithm extends this excellent behavior to multi-discharge recordings, markedly reducing error powers for this essential processing (Fig. 6).

When used in scanning-EMG signal processing, the median filter was found to distort the waveform of the signal. For this reason, although this filter is suitable for artifact detection, it is not the best option for signal restoration. The median filter tends to clip the peaks of the scanning signal if they are sharp [12, 13, 27, 5]. In addition, instead of the smooth profile of a physiological signal, signals processed with the median filter present a stepped amplitude profile in the spatial dimension [5]. In the present work, waveform distortion was observed when median filter-based methods were used to process multi-discharge scanning-EMG signals. Stepping in the spatial dimension was evident in signals processed with mean-median and median-median algorithms (Fig. 8 (a) and (b)). As a consequence of the distortion produced by the median filter, median filter-based algorithms have a higher error power than the MMLSS algorithm (Fig. 7).

The reason why spatial median filtering has been widely used to eliminate artifacts in scanning-EMG signals is because this type of averaging is very robust to outliers. Keeping this in mind, another option that could be considered for artifact removal is the use of a trimmed

mean to average in the discharge and in the spatial dimension. Note that this type of averaging, like the median, is also robust against outliers. In fact, trimmed mean has already been used in quantitative EMG as a method to extract representative MUP waveforms from MUP discharges [19, 21]. However, although the treatment of the outliers carried out by the trimmed mean and the median is effective, it can also be improved. These two algorithms are based on sorting the amplitude samples and then discarding a certain percentage of the data at both ends of the sorted set (in the case of the median, all the data except the central value). This is a blind criterion in the sense that it does not take into account what is the difference in amplitude between the sample values and the central tendency. On the other hand, the MMLSS algorithm first estimates the central tendency by obtaining a provisional processed signal (see section 2.1.1), and then detects outliers based on an amplitude difference criterion. Subsequently, the MMLSS algorithm reconstructs the noise-free scanning-EMG signal discarding the samples detected as outliers. This effective outlier detection is one of the reasons why the MMLSS has superior performance to any artifact removal method based on the median.

The suitability of processing multiple-discharge scanning-EMG recordings is evident because the improved scanning-EMG recording protocol proposed in [38, 28, 18] necessarily implies the recording of several discharges at each spatial position. Note that this new kind of recording allows to scan several MUs in a single insertion of the needle, implying a noticeable improvement over the original scanning-EMG. Additionally, processing recordings of more than one discharge makes it feasible to work at higher levels of muscle contraction, at least as long as the level of EMG activity is not so high as to prevent to correctly extract the firing of the MU from the trigger signal. Being able to work at higher levels of voluntary contraction is important because in this way it is possible to scan MUs that otherwise would not be active. Note that the additional artifact noise generated at a higher muscle contraction levels can be compensated for by recording and processing several discharges instead of only one. In the simulation experiments (Fig. 6), the error power of the MMLSS algorithm was similar when processing one discharge at 2% of MVC (median of P, -23.22 dBm) to when processing seven discharges at 4% of MVC (median of P, -23.31 dBm). In the same way, the error power was similar when processing one discharge at 4% of MVC (median of P, -14.2 dBm) to when processing five discharges at 8% of MVC (median of P, -15.85 dBm); and also, when processing one discharge at 8% of MVC (median of P, -8.87 dBm) to that for five discharges at 20% of MVC (median of P, -9.17 dBm). In summary, the effective elimination of artifacts by the

MMLSS algorithm facilitates working with multi-discharge scanning-EMG recordings, which in turn makes it easier to work at higher levels of voluntary contraction of muscle.

5-Conclusion

A new algorithm to remove artifacts from superimposed MUPs in scanning-EMG recordings has been proposed and evaluated. The method, based on the MLSS algorithm, is designed to process both single- and multi-discharge scanning-EMG signals. To test the algorithm, experiments were performed in different recording conditions, i.e., with different levels of muscle contraction, and with different numbers of discharges recorded at each scanning step. The results of these tests indicate that the algorithm adequately eliminates artifact noise while preserving the physiological waveform of the signal, and is more effective than any previously available algorithm at processing both single- and multi-discharge scanning-EMG signals.

Bibliography

[1]. Antoni, L., Stålberg, E. (1983). Scanning EMG data acquisition, processing and analysis. Electroencephalography and Clinical Neurophysiology, 56(3), S39-S40.

[2]. Artuğ, N. T., Goker, I., Bolat, B., Osman, O., Orhan, E. K., Baslo, M. B. (2018). New features for scanned bioelectrical activity of motor unit in health and disease. Biomedical Signal Processing and Control, 41, 109-128.

[3]. Borda, R. P., Frost Jr, J. D. (1968). Error reduction in small sample averaging through the use of the median rather than the mean. Electroencephalography and clinical neurophysiology, 25(4), 391-392.

[4]. Corera, Í., Malanda, A., Rodriguez-Falces, J., Porta, S., Navallas, J. (2017). Motor unit profile: a new way to describe the scanning-EMG potential. Biomedical Signal Processing and Control, 34, 64-73.

[5]. Corera, Í., Eciolaza, A., Rubio, O., Malanda, A., Rodríguez-Falces, J., Navallas, J. (2018). A masked least-squares smoothing procedure for artifact reduction in scanning-EMG recordings. Medical & Biological Engineering & Computing, 56(8), 1391-1402.

[6]. Dimitrov, GV., Dimitrova, NA. (1998). Precise and fast calculation of the motor unit potentials detected by a point and rectangular plate electrode. Med Eng Phys, Vol. 20, pp. 374–381.

[7]. Dioszeghy P (2002) Scanning electromyography. Muscle Nerve 25(S11):66–71

[8]. Farina, D., Fosci, M., Merletti, R. (2002). Motor unit recruitment strategies investigated by surface EMG variables. Journal of applied physiology, 92(1), 235-247.

[9]. Fuglevand, AJ., Winter, DA., Patla, AE. (1993) Models of recruitment and rate coding organization in motor-unit pools. J Neurophysiol, Vol. 70, pp. 2470-2488.

[10]. Goker, I., Baslo, M. B., Ertas, M., Ulgen, Y. (2009, September). Motor unit territories in juvenile myoclonic epilepsy patients. In 2009 Annual International Conference of the IEEE Engineering in Medicine and Biology Society (pp. 819-822). IEEE.

[11]. Goker, I., Baslo, B., Ertas, M., Ulgen, Y. (2010). Large motor unit territories by scanning electromyography in patients with juvenile myoclonic epilepsy. Journal of Clinical Neurophysiology, 27(3), 212-215.

[12]. Gootzen, T. H. (1990). Electrophysiological investigation of motor unit structure by means of scanning EMG. Muscle Fiber and Motor Unit Action Potentials. Katholieke Universiteit te Nijmegen, 89-106.

[13]. Gootzen, T. H., Vingerhoets DJ, Stegeman DF (1992) A study of motor unit structure by means of scanning EMG. Muscle Nerve 15(3):349–357

[14]. Hilton-Brown, P., Stålberg, E. (1983). The motor unit in muscular dystrophy, a single fibre EMG and scanning EMG study. Journal of Neurology, Neurosurgery & Psychiatry, 46(11), 981-995.

[15]. Hilton-Brown, P., Stålberg, E. (1983). Motor unit size in muscular dystrophy, a macro EMG and scanning EMG study. Journal of Neurology, Neurosurgery & Psychiatry, 46(11), 996-1005.

[16]. Hoke, M., Ross, B., Wickesberg, R., Lütkenhöner, B. (1984). Weighted averaging—theory and application to electric response audiometry. Electroencephalography and clinical neurophysiology, 57(5), 484-489.

[17]. Keenan KG, Valero-cuevas FJ (2007) Motor-unit function are most sensitive to neural properties. Journal of neurophysiology, 98:1581-1590.

[18]. Lapatki, B. G., Eiglsperger, U., Schindler, H. J., Radeke, J., Holobar, A., & van Dijk, J. P. (2019). Three-dimensional amplitude characteristics of masseter motor units and representativeness of extracted motor unit samples. Clinical Neurophysiology, 130(3), 388-395.

[19]. Leonowicz, Z., Karvanen, J., Shishkin, S. L. (2005). Trimmed estimators for robust averaging of event-related potentials. Journal of neuroscience methods, 142(1), 17-26.

[20]. Leski, J. M. (2002). Robust weighted averaging [of biomedical signals]. IEEE Transactions on Biomedical Engineering, 49(8), 796-804.

[21]. Malanda, A., Navallas, J., Rodriguez-Falces, J., Rodriguez-Carreño, I., Gila, L. (2015). Averaging methods for extracting representative waveforms from motor unit action potential trains. Journal of Electromyography and Kinesiology, 25(4), 581-595.

[22]. Mühler, R., Specht, H. V. (1999). Sorted averaging-principle and application to auditory brainstem responses. Scandinavian audiology, 28(3), 145-149.

[23]. Nandedkar, S. D., Sanders, D. B. (1989). Median averaging of electromyographic motor unit action potentials: comparison with other techniques. Medical and Biological Engineering and Computing, 27(6), 566-571.

[24]. Navallas, J., Sta, E. (2009). Studying motor end-plate topography by means of scanning-electromyography. Clinical Neurophysiology, 120(7), 1335-1341.

[25]. Navallas J, Malanda A, Gila L, Rodríguez-falces J, Rodríguez I (2010) A muscle architecture model offering control over motor unit fiber density distributions. Med Biol Eng Comput 48(9):875–886

[26]. Rodríguez I, Malanda A, Gila L, Navallas J, Rodríguez-Falces J (2006) Filter design for cancellation of baseline-fluctuation in needle EMG recordings. Comput Methods Programs Biomed 81(1):79–93

[27]. Navallas J, Stålberg E, Rodríguez-falces J (2012) Scanning electromyography. In: Schwartz M (ed) EMG methods for evaluating muscle and nerve function. INTECH Open Access Publisher

[28]. Navallas, J., Eciolaza, A., Rubio, O., Corera, Í., Rodríguez-Falces, J. & Malanda, A. (2018). Single-needle multiscanning-EMG. Proceedings of the XXII Congress of the International Society of Electrophysiology and Kinesiology (ISEK).

[29]. Falces, J. R., Trigueros, A. M., Useros, L. G., Carreño, I. R., Irujo, J. N. (2006). Modeling fibrillation potentials-a new analytical description for the muscle intracellular action potential. IEEE transactions on biomedical engineering, 53(4), 581-592.

[30]. Schnetzer MA, Ruegg DG, Baltensperger R, Gabriel JP (2001) Three-dimensional model of a muscle and simulation of its surface EMG. In: Proceedings of the 23rd annual international conference of the IEEE engineering in medicine and biology society, 2001, vol 2. IEEE, pp 1038–1043

[31]. Stålberg, E., Antoni, L. (1980) Electrophysiological cross section of the motor unit. J. Neurol. Neurosurg. Psychiatry, 43: 469-474.

[32]. Stålberg, E., Chu, J., Bril, V., Nandedkar, S., Stålberg, S., Ericsson, M. (1983). Automatic analysis of the EMG interference pattern. Electroencephalography and clinical neurophysiology, 56(6), 672-681.

[33]. Stålberg E (1985) Single fiber EMG, macro EMG, and scanning EMG. New ways of looking at the motor unit. CRC Crit Rev Clin Neurobiol 2(2):125–167

[34]. Stålberg, E., Eriksson, P. O. (1987). A scanning electromyographic study of the topography of human masseter single motor units. Archives of oral biology, 32(11), 793-797.

[35]. Stålberg, E., Dioszeghy, P. (1991). Scanning EMG in normal muscle and in neuromuscular disorders. Electroencephalography and Clinical Neurophysiology/Evoked Potentials Section, 81(6), 403-416.

[36]. Stålberg, E., Falck, B., Sonoo, M., Stålberg, S., Åström, M. (1995). Multi-MUP EMG analysis—a two year experience in daily clinical work. Electroencephalography and Clinical Neurophysiology/Electromyography and Motor Control, 97(3), 145-154.

[37]. Strutz, T. (2010) Data fitting and uncertainty: a practical introduction to weighted least squares and beyond. Vieweg and Teubner, Berlin

[38]. Van Dijk, JP., Eiglsperger, U., Hellmann, D., Giannakopoulos, NN., McGill, KC., Schindler, HJ., et al (2016). Motor unit activity within the depth of the masseter characterized by an adapted scanning EMG technique. Clin Neurophysiol; 127:3198–204.

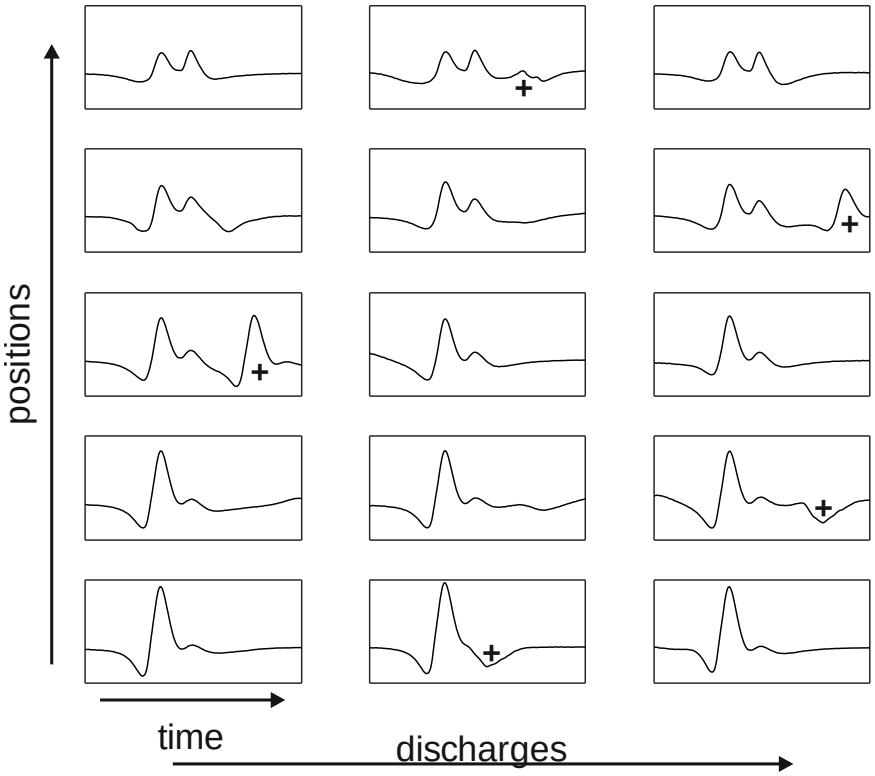

Fig. 1. Representation of all MUP discharges recorded at five consecutive positions in a scanning-EMG signal. Note that three discharges are recorded at each position. The horizontal and vertical axis represent the discharge and spatial dimension respectively. Each MUP discharge is a signal that varies with time. Note that evident artifacts are present in the locations marked with a cross (+).

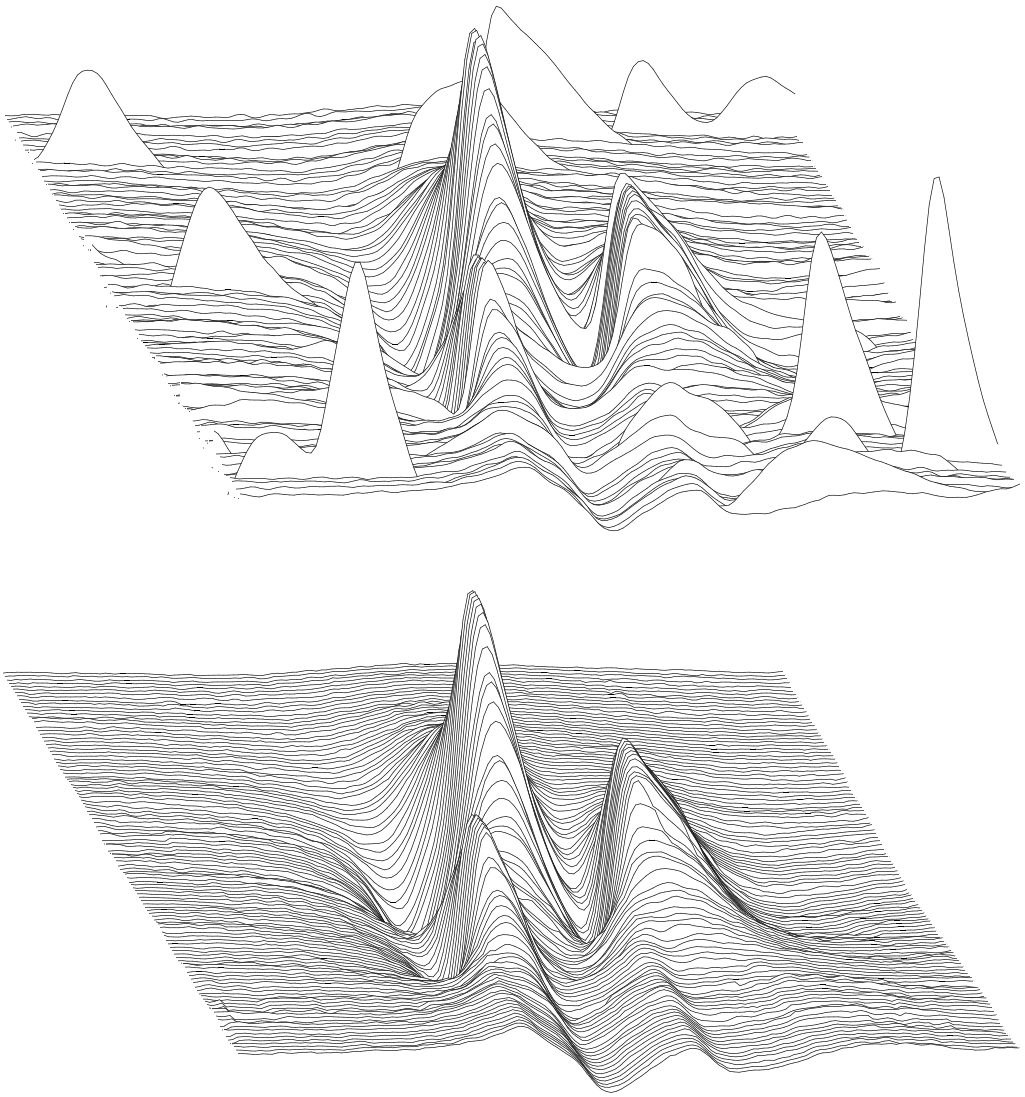

Fig. 2. Three-dimensional representation of a single-discharge scanning-EMG signal: (a) raw signal, in which there are artifacts, i.e. activity that is not synchronized with the recorded MUP; (b) after applying a spatial median filtering algorithm.

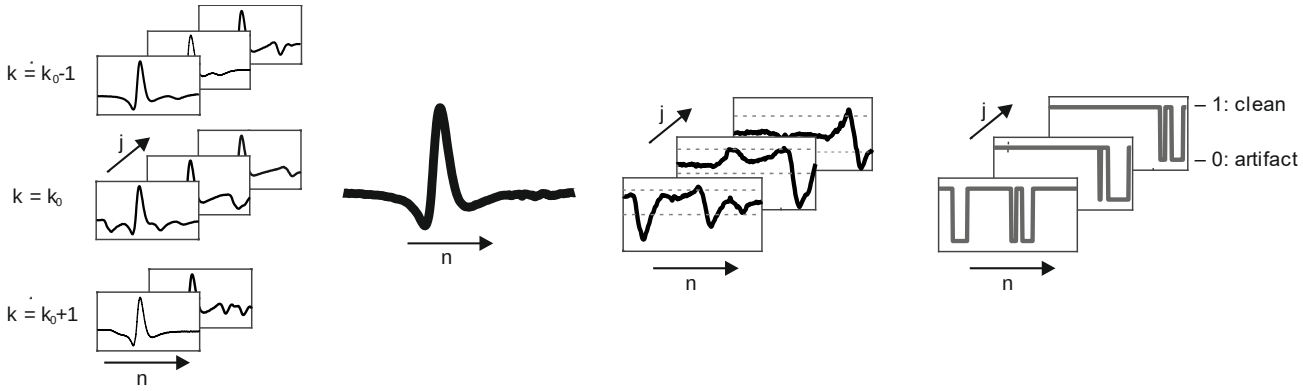

Fig. 3. (a) The scanning-EMG signal at the input of the algorithm comprises a set of different discharges at each recording position k. In the figure, the discharges corresponding to the positions $k_0 - 1$, k_0 and $k_0 + 1$ are shown; (b) the median of all discharges contained in the positions $k_0 - 1$, k_0 and $k_0 + 1$ (the median filter order, L, is 3); (c) the difference between the input discharges and the median-filtered signal in the position k_0. The dashed lines represent the positive and negative threshold respectively; (d) validity mask values associated with the different discharges at position k_0. Note that 1 corresponds to a valid sample and 0 to a non-valid one.

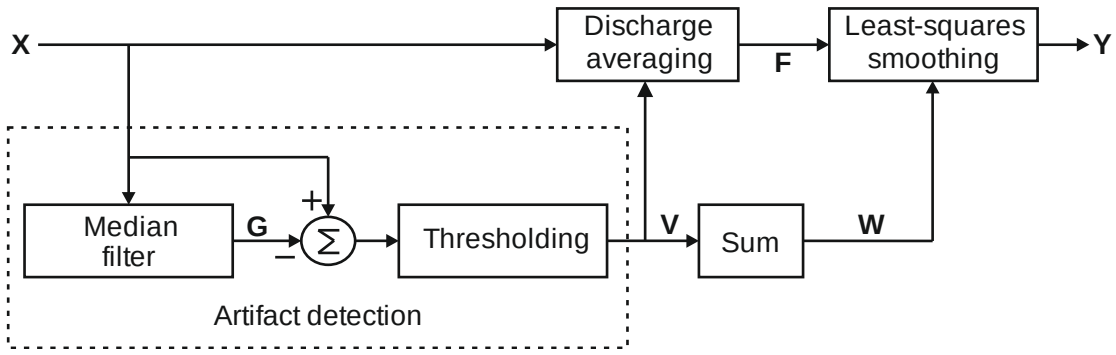

Fig. 4. Block diagram showing the steps of the MMLSS algorithm. In a first main step (boxed with a dashed line), the artifact-free samples of the input signal, $\boldsymbol{X}$, (which is the complete data for each set of discharges at each recording position) are determined by calculating a validity mask, $\boldsymbol{V}$. To calculate $\boldsymbol{V}$ a signal, $\boldsymbol{G}$, is prepared by applying a double median filter to the input signal $\boldsymbol{X}$. The signal $\boldsymbol{G}$ is then subtracted from $\boldsymbol{X}$, and this difference is thresholded to give the validity mask, $\boldsymbol{V}$. After that, the different discharges contained in $\boldsymbol{X}$ at each position are weight-averaged using the validity mask values, $\boldsymbol{V}$, as weights, so that an averaged signal, $\boldsymbol{F}$, is obtained based on the information of valid samples only. Also, an overall validity mask, $\boldsymbol{W}$ is obtained by summing at each position the different values of the validity mask $\boldsymbol{V}$ associated with the different discharges. In the last step, the output of the algorithm, $\boldsymbol{Y}$, is calculated by applying a

least-squares smoothing procedure to the averaged signal $\boldsymbol{F}$ along the spatial dimension, using the overall validity mask values $\boldsymbol{W}$ as weights.

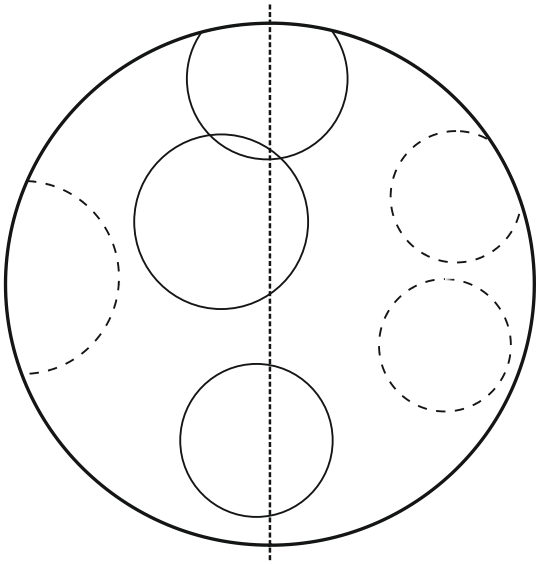

Fig. 5. Schematic representation of a cross section of simulated muscle. The MU territories of active MUs are represented by circles, and the corridor through which the electrode passes, by a dashed vertical line. Only signals corresponding to active MUs whose territory is traversed by the scanning corridor (solid line circumferences) were simulated.

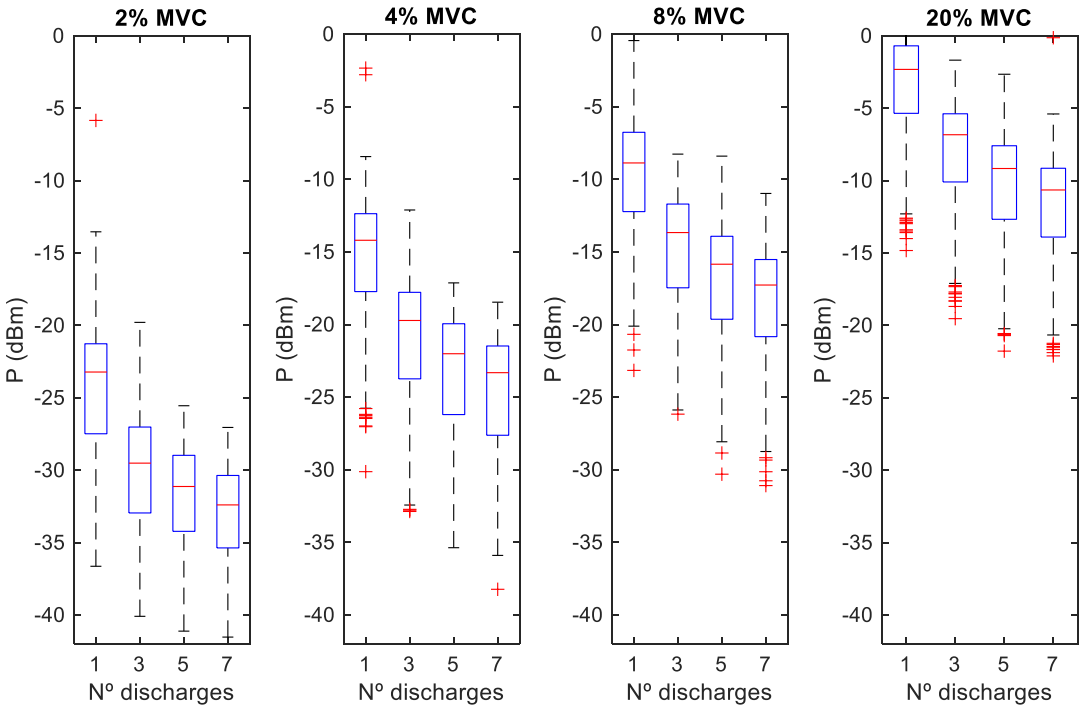

Fig. 6. Boxplot representation of the error power, P, of the signals processed with the MMLSS algorithm for different number of discharges and different percentages of MVC; (a) 2% MVC; (b) 4% MVC; (c) 8% MVC; (d) 20% MVC.

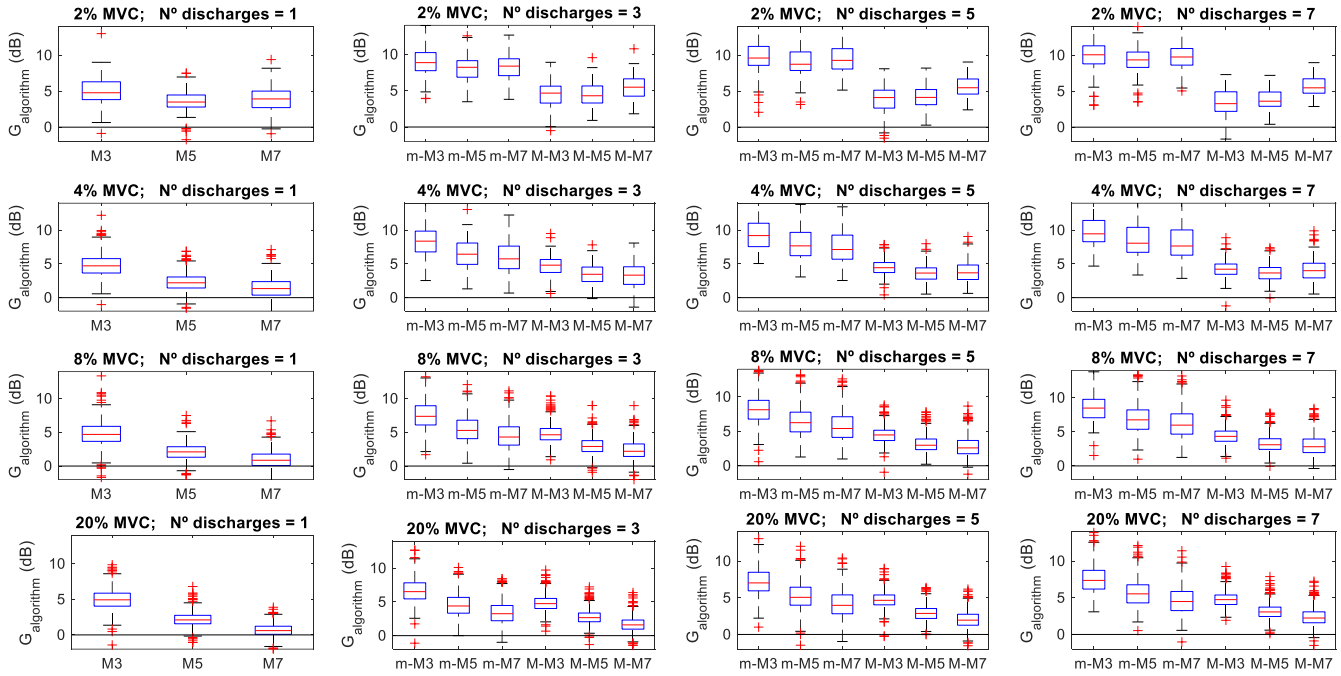

Fig. 7. Boxplot representation of the gain, $G_{algorithm}$, of the MMLSS algorithm with respect to the other algorithms for different levels of muscle contraction and for different numbers of discharges. The other algorithms studied were: the 3-point-mean-median (m-M3), the 5-point-mean-median (m-M5), the 7-point-mean-median (m-M7), the 3-point-median-median (M-M3), the 5-point-median-median (M-M5), the 7-point-median-median algorithm (M-M7) for multi-discharge scanning signals; and the 3-point-median (M3), the 5-point-median (M5) and the 7-point-median algorithm (M7) for single-discharge scanning signals.

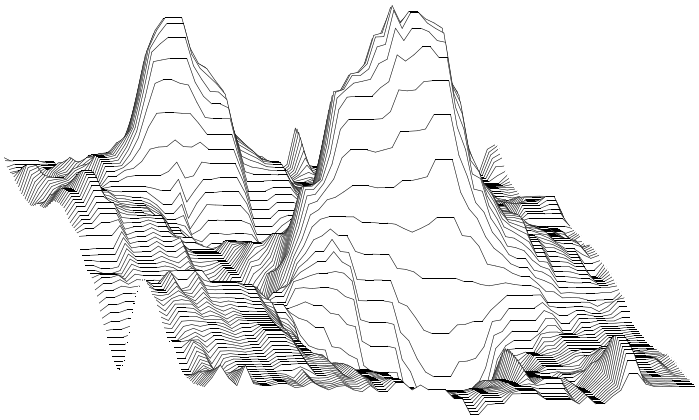

585

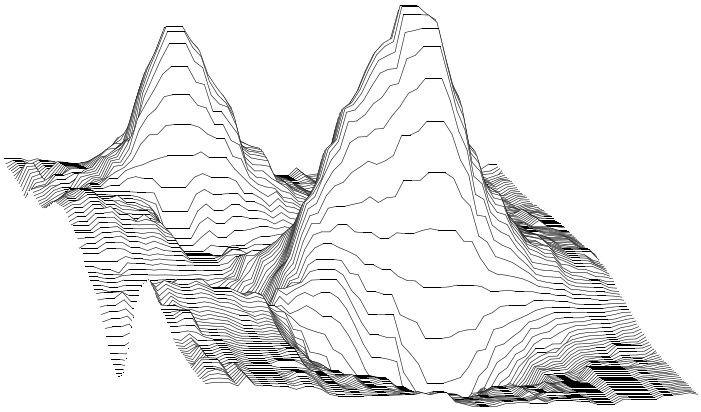

586

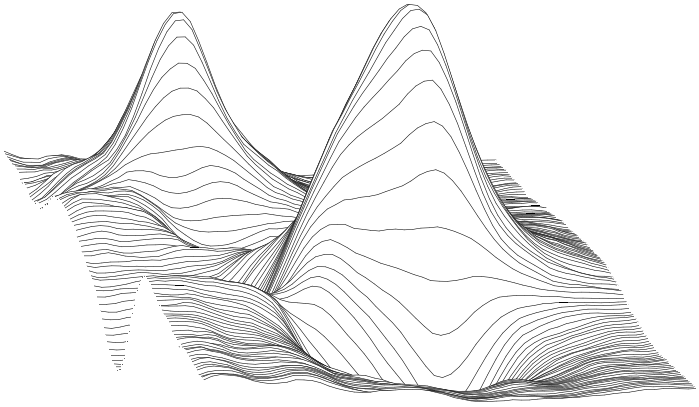

587

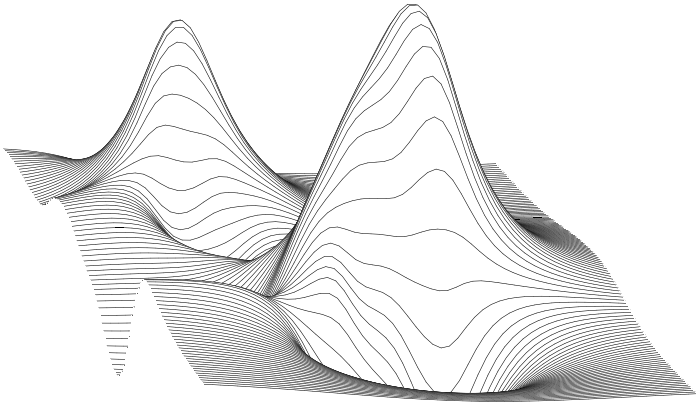

588

Fig. 8. Simulated scanning-EMG signal processed using different algorithms: (a) 5-point-Mean-median, P = -14.52 dBm; (b) 5-point-Median-median, P = -18.68 dBm; (c) MMLSS, P = -22.04 dBm; (d) Ideal noise-free signal.

Authors' Biographies

Íñigo Corera obtained his MSc in Telecommunication Engineering in 2014. He is PhD student in the UPNA and his research fields include analysis and processing of EMG signals and optimization algorithms.

Javier Navallas obtained his PhD in 2008. He is Associate Professor in the UPNA. His research interests are biomedical signal processing, modeling of the neuromuscular systems and neural information processing.

Armando Malanda received his PhD in 1999. He is Associate Professor in the UPNA. His areas of interest comprise the analysis, modeling and simulation of bioelectrical signals, particularly EEG and EMG.

Javier Rodríguez-Falces obtained his PhD in 2007. He is Associate Professor in the UPNA. His research interests include modeling and analysis of muscle electrical and mechanical responses and neuromuscular adaptations to exercise.